The evaporation of a salty film

Rob Style

March 15, 2007

1 Introduction

Evaporation of water is an important phase transformation that appears in many guises throughout everday life. Its effects range from processes intrinsically involved in the atmospheric water cycle, to the regulation of body temperature in hot environments, the production of coffee ring stains beneath a spilt coffee droplet and to important processes underlying microfluidics.

Although evaporation as a pure bulk phase transformation is well understood, when one adds solutes to the liquid, or brings the liquid into contact with a substrate, we obtain a new and rich variety of possible behaviours that we can access experimentally and analyse theoretically.

A well known example of is the effect of combining a solute with evaporation is given by the 'tears of wine' phenomenon [1],[2]. When one swills a glass of wine, a liquid film is produced up the side of the glass above the bulk liquid. Alcohol evaporates more rapidly in the film away from the bulk wine, and the film becomes depleted of alcohol. This depletion decreases the surface concentration of the film relative to that of the bulk wine, leading to a gradient in surface energy. This gradient causes a marangoni flow, drawing liquid up into the film above the bulk wine. Eventually, enough liquid is drawn up into the film that it becomes unstable to gravity and falls–like a tear of wine. Any gradient in surface temperature or concentration will cause Marangoni flows, and thus marangoni flows can be extremely important in the presence of phase transitions, particularly evaporation.

A second complexity is introduced by the addition of a substrate into the problem [3]. Although the wetting of substrates has been well studied [4], there are still many interesting phenomena associated with the evaporation of films that have only recently received attention, such as the investigation of coffee ring formation by a sessile, particle–laden droplet [5], the observations of a finite contact angle in an evaporating wetting film [6], and of particular interest, the experiments of Du and Stone on evaporatively grown salt trees [7].

Neufeld has recently performed a series of experiments observing the evaporation of a sessile, salty droplet (private communication). Although simple in nature, the experiments show several key features that we wish to understand (see Fig. 1). Namely:

- Overturning of liquid in the bulk

- Salt crystal deposition in the bulk, initiating at the outer edge

- Formation of a thin, rough salt crystal film beyond the edge of the bulk droplet

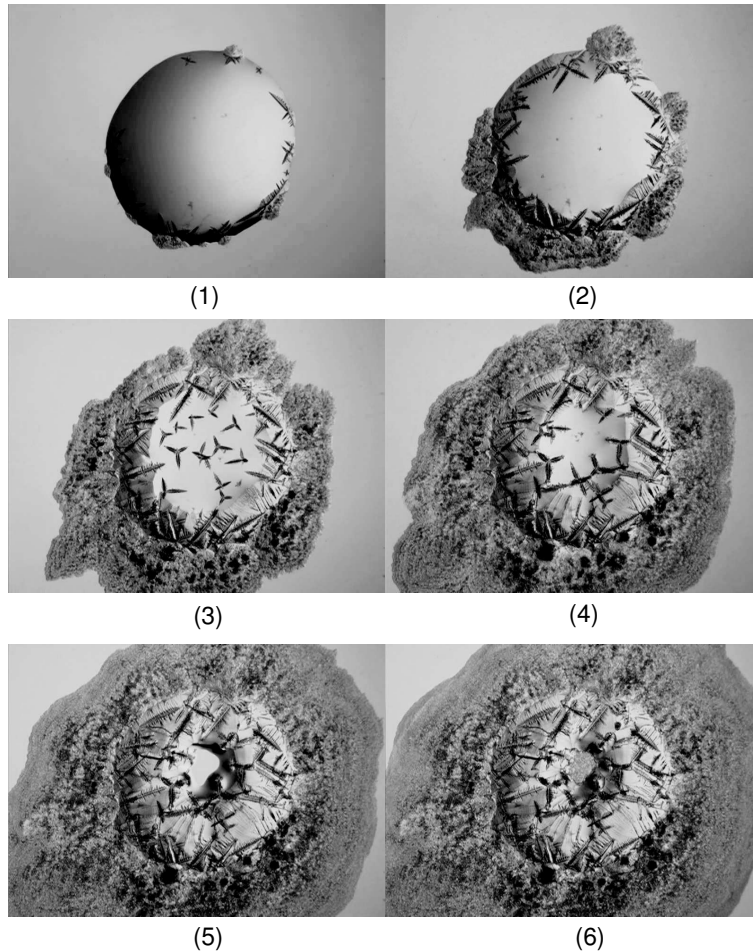- Continual growth of the outer limit of this thin salt film

Figure 1: Plan view of the evaporation of a 5μl droplet of saturated NH_4Cl solution. Room temperature is $22°C$ and relative humidity is 42%. The images are shown at approximately six minute intervals. (1) Just post commencement of the experiment: some salt is observed at the edge of the droplet when evaporation is highest. (2) Precursor film growth observed around droplet. (3) Some dendritic growth observed in the bulk droplet: these crystals are effected by flow in the droplet. (4) Bulk liquid reduces in radius while precursor film continues to spread. (5) Dewetting occurs at the centre of the droplet and hence bulk liquid is no longer exposed to air. (6) Precursor film continues to grow and dewetted area covered in growth similar in appearance to outlying precursor growth.

In this work, we will demonstrate the basic processes at work in the evaporation of a salty droplet by way of simplified models and show that the above observations stem from

the combined action of these processes. In this way, we will be able to understand the processes important for the growth of evaporatively grown salt trees which we aim to study in later work. For the current study, of most interest is the creation of the salt crystal under and beyond the edge of the bulk droplet. Vapour transport of salt cannot account for the deposition beyond the confines of the bulk droplet, so we ascribe the presence of the salt to the evaporation of a thin film of liquid fed by Marangoni flow from the bulk droplet. We will see that the growth of the salt–crystal from this film is subject to a new instability associated with the development of supersaturation at the liquid–vapour boundary.

We describe the mechanism for this new instability as follows. A thin film of constant salt concentration sits atop a planar salt crystal with which it is in equilibrium. The vapour pressure in the surrounding atmosphere is reduced so that evaporation occurs from the surface of the film and so that salt previously dissolved in the evaporated portion of liquid is rejected into the surface layer of the film (salt having effectively zero partial pressure in the vapour phase). This causes supersaturation at the liquid–vapour interface that diffuses towards the solid–liquid interface. In this manner, salt will be transported from the liquid–vapour interface to deposit upon the salt crystal. However, as the salt crystal will be growing into an increasing supersaturation, the interface will be unstable to small perturbations.

In many aspects, this salt precipitation is similar to the unstable solidification front of a salt freezing from a binary alloy [8]. For comparison, we briefly review the theory of constitutional supercooling.

Imagine a pure, planar salt crystal, growing from a binary alloy (water and salt). We set the far field composition and temperature of the alloy to be c_∞ and T_∞ respectively, and assume that the liquidus relationship between concentration c and temperature T is approximately linear so that

$$T_L(c) = mc + T_0. \tag{1}$$

Then $T_L(c_\infty) < T_\infty$ so that the far field liquid is not supercooled. Also, the temperature at the solid–liquid interface $T_i < T_\infty$ is such that the solid is in equilibrium with the surrounding liquid so that we must have $T_i = T_L(c_i)$.

Now, in front of the advancing salt front, water must be being rejected so that $c_i < c_\infty$. Thus we will see solutal and thermal boundary layers in front of the advancing front, across which the salt and temperature respectively will vary between their interface and far field values. The diffusivity of heat κ is much larger than the diffusivity of salt in water D_s, and so the thermal boundary layer will be thicker than the solutal boundary layer. If we translate the solutal concentration into the equilibrium liquidus temperature in the liquid from Eq.(1), we then see (Fig. 2) that this implies that there will be a region directly ahead of the advancing solid front where the liquid is at a temperature below the liquidus if

$$\left.\frac{\partial T}{\partial z}\right|_{\mathrm{sl}} < m \left.\frac{\partial c}{\partial z}\right|_{\mathrm{sl}}. \tag{2}$$

This 'constitutional supercooling' is produced by rejection of solvent in front of the solidification front, and it is well known that the front is unstable to small perturbations [9] leading to dendritic growth as has been observed experimentally, for example in the case of ammonium chloride, by Huppert [10].

Therefore in both situations, we produce salt from a binary alloy of salt and water. Also in both cases, there is a local increase of the free energy of the system above the
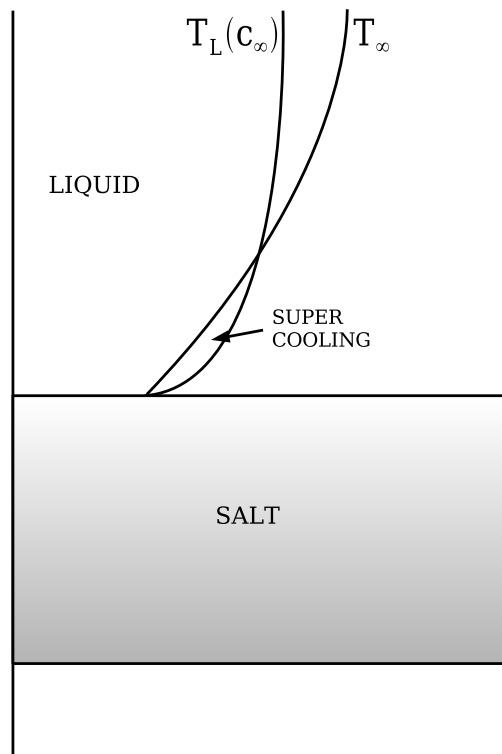
Figure 2: Diagram demonstrating the origin of constitutional supercooling at the salt–liquid interface (cf principle lectures by MGW for added details).
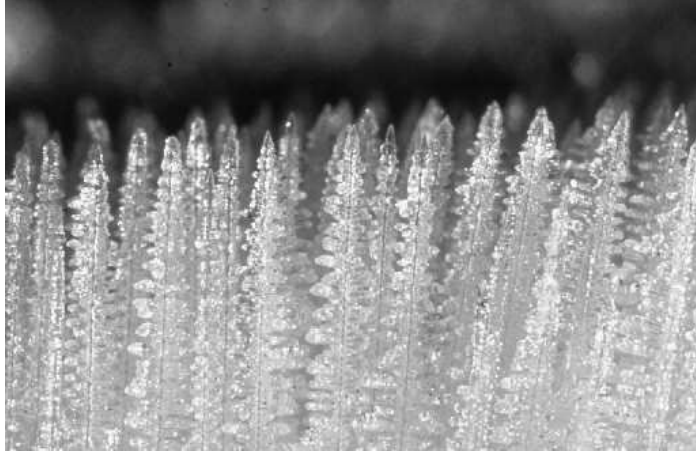
Figure 3: Close up of salt dendrites at the surface of a mushy layer advancing into ammonium chloride solution [10].

equilibrium value (supersaturation/supercooling) which drives the salt–liquid interface to become unstable. One final similarity is that in both situations convection can occur due to density differences associated with gradients in temperature and concentration. However, the key difference lies in the fact that constitutional supercooling is caused by water rejection at the salt crystal boundary, and is always immediately relieved by immediate solidification upon the salt crystal. However in the evaporative case, supersaturation is produced at some distance, namely the film thickness, away from the deposited salt crystal and therefore leads to differing growth behaviour and the possibility of homogeneous nucleation of salt at the liquid–vapour interface for rapid enough evaporation rates. The simple observation that the crystal forms produced by both processes vary significantly (Fig. 3) tells us that this difference is important in determining growth characteristics, and thus worthy of study.

2   Model of an evaporating film

In order to wade through the mire of ccompeting processes involved in producing the complex patterns seen experimentally, we begin by considering a simple modelconsisting of a planar salt interface, covered with a film of uniform thickness d In this manner we can systematically study the most important physical mechanisms at play. We can control the water vapour pressure P_∞ in the surrounding atmosphere and so initially we choose a vapour pressure such that the water in the film is in equilibrium with the water vapour and the film has uniform concentration c_L in equilibrium with the underlying salt crystal. We then reduce P_∞ so evaporation occurs at the liquid–vapour interface at a rate E where E is measured in volume per second per unit area of surface.

At this point it is useful to make explicit the assumptions that we make in order that we may justify them later:

- Because of the disparity between solutal and thermal diffusivities, thermal effects are neglected in the dynamics of the system.
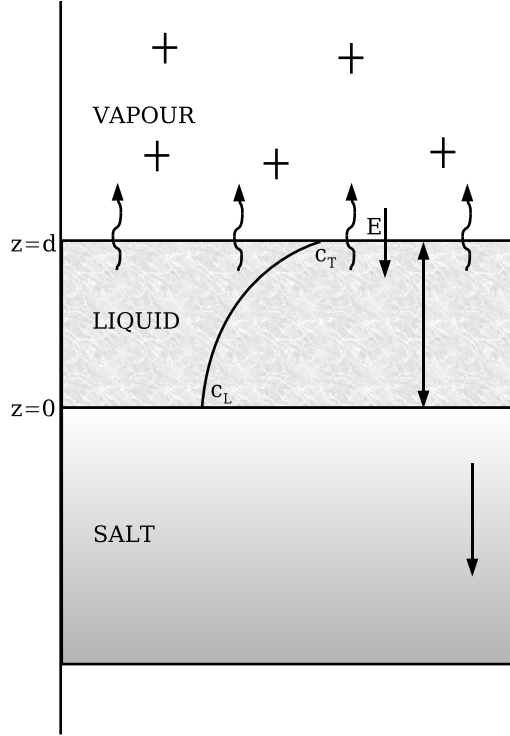
208

Figure 4: Schematic diagram for the evaporation of a film of salty liquid

- The film is of uniform thickness, and vapour pressure over the film is constant so that there is no marangoni flow feeding the film,

- The salt concentration is sufficiently low that the advection–diffusion equations hold,

- The addition of salt to a volume of liquid does not change the volume: $\rho_l(c)$ =const.

Therefore we have a film as shown in Fig.(4), in the frame of reference of the liquid–vapour interface. In the liquid, the concentration of the salt satisfies the diffusion–advection equation, so that we have

$$\frac{\partial c}{\partial t} - E\frac{\partial c}{\partial z} = D_s \nabla^2 c, \tag{3}$$

which we can nondimensionalise by scaling times with d_0/E and lengths with d_0, where d_0 is the initial thickness of the quasi–stationary film, to give

$$\mathrm{Pe}\left[\frac{\partial c}{\partial \tilde{t}} - \frac{\partial c}{\partial \tilde{z}}\right] = \tilde{\nabla}^2 c, \tag{4}$$

where nondimensional variables are denoted by a tilde, and the effective Peclet number $\mathrm{Pe} = d_0 E/D_s$ is the ratio of evaporation to diffusion rates. A natural starting point in the analysis of the phenomenon is therefore to select a small Peclet number by choosing a slow evaporation rate (or sufficiently small film). We will then use a quasi–stationary approximation so that $d \approx d_0$ throughout the analysis.

As boundary conditions for the problem, there are several natural conditions arising from the formulation. These consist of equilibrium at the solid–liquid interface

$$c|_{sl} = c_L + \mathcal{C}\mathcal{K}_{sl}, \tag{5}$$

conservation of salt at the solid–liquid interface

$$D_s \frac{\partial c}{\partial z}\bigg|_{sl} = (V + \dot{h})c_{salt}, \tag{6}$$

thinning of the film

$$\dot{d} = -E, \tag{7}$$

and conservation of salt at the liquid–vapour interface

$$D_s \frac{\partial c}{\partial z}\bigg|_{lv} = Ec_T, \tag{8}$$

where we define $\mathcal{K}_{sl}$ to be the curvature of the solid–liquid interface, $\mathcal{C}$ to be the Gibbs–Thomson coefficient for the equilibrium salt concentration (see Appendix A), V is the growth velocity of the salt crystal, h is the height of the crystal surface, and c_T and c_{salt} are the salt concentrations at the liquid–vapour interface and in the salt crystal respectively.

We will require one more boundary condition to complete the set of equations, and this will come from the relationship between the evaporation rate E, the concentration at the liquid–vapour interface c_T and far field vapour pressure P_∞. The evaporation rate will depend upon the dynamics of the vapour, in that the transport of water vapour from the interface will be determined by the water vapour gradient at the liquid–vapour interface

$$D_w \frac{\partial P_{wv}}{\partial z}\bigg|_{lv} = E, \tag{9}$$

where D_w is the diffusivity of water vapour in air and P_{wv} is the local water vapour pressure. Therefore to obtain the water vapour pressure profile for a steady diffusion of vapour in a background of air, we must solve Laplace's equation in the vapour with boundary conditions $p(\infty) = P_\infty$ and

$$P_{lv} = P_0(1 - c_T), \tag{10}$$

where P_0 is the vapour pressure at pure equilibrium, and c_T is the concentration of salt at the film surface (see Appendix B). For pure evaporation, these boundary conditions reduce to constant values at the surface of the droplet and in the far field, and so good approximations to the evaporation rate can be made by assuming simple geometries for the droplet [5],[11]. For fast evaporation rates, there is a jump in vapour pressure from the equilibrium vapour pressure, given by Eq.(10) that will be controlled by the Hertz–Knudsen relationship, which written as the boundary conditions will add some detail to the form of the flow. However in this paper, since E is an experimentally controllable parameter, we will assume constant evaporation rate.

For small Peclet number, the diffusion–advection equation reduces to Laplace's equation, and so the solutal field in the film for planar growth is given by

$$c \approx (c_T - c_L)\frac{z}{d} + c_L. \tag{11}$$

210

Applying boundary condition (8) gives

$$c_T = \frac{c_L}{1 - \mathrm{Pe}} \tag{12}$$

and so the rate of growth of the solid is given by

$$V = E \frac{c_T}{c_{salt}}. \tag{13}$$

This agrees with our intuition, because for the small Peclet number limit, information is diffused rapidly across the film, and so we expect evaporation to occur simultaneously with salt precipitation. Equation (13) demonstrates that if we evaporate a layer of water of thickness δd, simultaneously an amount of salt equivalent to the salt dissolved in δd is precipitated corresponding to instantaneous diffusion.

We are now in a position to conduct a quasi–stationary linear stability analysis of the film. In the film, there is a slow time dependence of the basic state given by $O(\dot{c}/c_L) \sim \mathrm{Pe}E/d$. We will impose a perturbation upon the solid–liquid interface which will grow on a faster timescale (that we can check *a posteriori*). Therefore we designate slow and fast timescales as $(\mathrm{Pe}E/d)t = t^*$ and $(E/d)t = \tau$ respectively so that

$$\frac{\partial}{\partial t} = \frac{\partial}{\partial t^*} + \frac{\partial}{\partial \tau}.$$

We label the linear, quasi-stationary state given by Equation (11) as $c_0(z, t^*)$, and impose a dimensionaless perturbation with a fast timescale upon the solid–liquid interface

$$h = \tilde{h} e^{ik\tilde{x} + \sigma\tau}. \tag{14}$$

We assume a form

$$c(\tilde{z}, \tau, t^*) = c_0(z, t^*) + \tilde{c}(\tilde{z}, t^*) e^{ik\tilde{x} + \sigma\tau}. \tag{15}$$

Then the diffusion advection equation (3) in the frame of reference of the solid–liquid interface becomes

$$\mathrm{Pe}^2 \frac{\partial}{\partial t^*} \left(c_0 + \tilde{c} e^{ik\tilde{x} + \sigma\tau} \right) + \mathrm{Pe}\sigma \tilde{c} e^{ik\tilde{x} + \sigma\tau} = \frac{\partial^2 c_0}{\partial \tilde{z}^2} + \left[\frac{\partial^2 \tilde{c}}{\partial \tilde{z}^2} - k^2 \tilde{c} \right] e^{ik\tilde{x} + \sigma\tau}, \tag{16}$$

which in the small Peclet number limit, reduces to

$$\frac{\partial^2 \tilde{c}}{\partial \tilde{z}^2} - k^2 \tilde{c} = 0, \tag{17}$$

and has solution

$$\tilde{c} = A \sinh k\tilde{z} + B \cosh k\tilde{z}. \tag{18}$$

Applying boundary conditions in the small Peclet number limit, we obtain

$$A = -\tilde{h} \tanh kd \left[\frac{\mathcal{C}}{d} k^2 + \mathrm{Pe} \frac{c_L}{1 - \mathrm{Pe}} \right]$$

and

$$B = \tilde{h} \left[\frac{\mathcal{C}}{d} k^2 + \mathrm{Pe} \frac{c_L}{1 - \mathrm{Pe}} \right],$$

Table 1: Table of typical values for the ammonium chloride/water system at $T = 20°C$

Constant	Value	Units
c_L	27.2	wt%
γ_{sl}	5×10^{-2}	$\mathrm{J\,m^{-2}}$
μ	1.787×10^{-3}	$\mathrm{kg\,m^{-1}\,s^{-1}}$
R	8.314	$\mathrm{J\,K^{-1}\,mol^{-1}}$
m	4.79	$\mathrm{K\,wt\%^{-1}}$
D_s	10^{-9}	$\mathrm{m^2\,s^{-1}}$
$\frac{\partial \gamma}{\partial c}$	4×10^{-4}	$\mathrm{kg\,s^{-2}\,wt\%^{-1}}$
ρ_s	5.6×10^4	$\mathrm{mol\,m^{-3}}$
$\mathcal{C}$	-7×10^{-9}	$\mathrm{wt\%\,m}$
E	10^{-7}	$\mathrm{m\,s^{-1}}$

so that applying the Equation (6) for the conservation of salt at the solid–liquid interface, we find the dimensional dispersion relationship

$$\sigma = \frac{1}{c_{salt}} k \tanh kd \left[E c_L + D_s \mathcal{C} k^2 \right]. \tag{19}$$

For relatively short wavelengths, we can approximate this as

$$\sigma = \frac{k}{100} [E c_L + D_s \mathcal{C} k^2], \tag{20}$$

as is plotted in Fig.(5).

Using typical values from Table (1), we find from Eq.(20) that the cutoff wavenumber $k_c = 6.2 \times 10^5 \mathrm{m^{-1}}$, so that the small wavelength approximation is justified. The maximum growth rate can also be derived from Eq.(20), and we find that $k_{max} = 3.57 \times 10^5 \mathrm{m^{-1}}$ and $\sigma_{max} = 6.4 \times 10^{-3} \mathrm{s^{-1}}$ corresponding to a time period of around 3 hours. For this instability to be relevant, we require that the growth rate be faster than the rate of thinning of the film, so that $E/d < \sigma_{max}$ and we find that $d > 1.5 \times 10^{-5} \mathrm{m}$. Therefore we expect that in the precursor film (typically around a micron thick), with these conditions, the instability will not have time to develop, unless there is a flow of liquid in to replace evaporated material. We must also remember that for a sufficiently thin film such as the precursor film, electrostatic forces will retard the evaporation rate of the film, and so for a full treatment, we will need to include these effects.

We note that for $E \sim 10^{-7} \mathrm{m\,s^{-1}}$, the Peclet number is $d \times 10^2$, and so for most natural situations, the Peclet number will be reasonably small. We also note that when the film is sufficiently thick, convection of the film will set in due to the increase in density at the surface of the film, and the stationary approximation of the liquid in the film will no longer be valid.
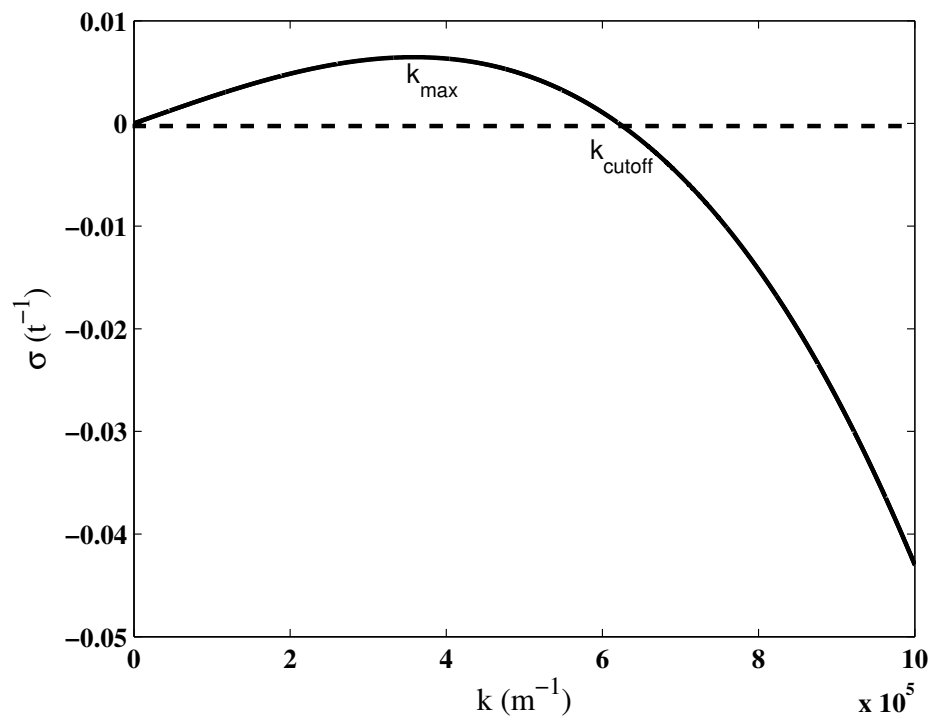
Figure 5: Plot of growth rate against wavenumber for small Peclet number.

3   Large Peclet number

When the evaporation rate is sufficiently high, or the film is sufficiently thick, the rate of diffusion of salt across the film becomes small relative to the thinning rate of the film. This means that there will be a solutal boundary layer at the liquid–vapour interface with on some time scale, the salt–liquid interface unaware of the presence of evaporation at the upper surface.

Therefore, in the frame of reference of the liquid–vapour interface, the diffusion–advection equation for salt concentration becomes

$$\frac{\partial c}{\partial t} - E\frac{\partial c}{\partial z} = d\frac{\partial^2 c}{\partial z^2}, \tag{21}$$

so that before the diffusive information reaches the salt–liquid interface, the profile will satisfy the time independent form of Eq.(21) so that

$$c = c_L + (c_T - c_L)\left[\frac{e^{\frac{E(z+d)}{D_s}} - 1}{e^{\frac{dE}{D_s}} - 1}\right]. \tag{22}$$

Applying Eq.(6) for the conservation of mass at the liquid-vapour interface, we find that

$$c_T = c_L e^{\text{Pe}} \tag{23}$$

which, we note gives the same result as for the small Peclet number case (Eq.(12)) when we take the small Peclet number limit of this expression. From this expression, we notice that the surface value of the salt concentration in the film will increase very rapidly with Peclet number. Therefore, there will be some value of the Peclet number above which the concentration at the liquid–vapour interface is sufficiently high to cause homogeneous nucleation.

In order to estimate the critical Peclet number above which homogeneous nucleation will occur, we need to calculate the energy required to create a critical nucleus of salt from solution.

The free energy change associated with creating a nucleus of radius r of salt from salt solution is

$$\Delta G = \gamma_{sl}4\pi r^2 + [\mu_s(T, P_s) - \mu_l(T, P_l, c)]\frac{4}{3}\pi r^3, \tag{24}$$

where the first term on the right hand side stems from the energy change required to create a solid–liquid surface between the two phases, and the second term is the change in free energy associated with the change of phase.

Expanding the chemical potentials of the two phases about equilibrium, we have

$$\mu_s(T, P_s) - \mu(T, P_l, c) = -RT\ln(c/c_L), \tag{25}$$

and therefore

$$\Delta G = \gamma_{sl}4\pi r^2 - RT\ln(c/c_L)\frac{4}{3}\pi r^3. \tag{26}$$

214

As can be seen, this free energy change has a maximum at $r = r^*$, so that if $r < r^*$, the nucleus will shrink to zero and if $r > r^*$, the nucleus will diverge and homogeneous nucleation occurs. The critical energy is therefore

$$\Delta G(r^*) = \frac{16\pi\gamma_{sl}^3}{\rho^2 R^2 T^2 \ln(c/c_L)}.\tag{27}$$

For homogeneous nucleation to occur, the thermal fluctuations in the film must be large relative to the critical free energy of nucleation. This means that the Gibbs number $g = \Delta G(r^*)/kT$ must be smaller than $O(100)$ for nucleation to occur [12] (note that this estimate will depend upon the nature of the system). Approximating $c/c_L = e^{\mathrm{Pe}}$ from Eq.(23), we thus obtain that

$$\mathrm{Pe} \leq 1\tag{28}$$

for no homogeneous nucleation, and so the large Peclet number case is unviable.

We note that for intermediate Peclet number, we cannot treat the profile as quasi–stationary, and so a full treatment of the instability will require a numerical evaluation of the instability from the initial conditions, or otherwise a modified model. One possibility would be to assume a flow perpendicular to the plane of the instability that maintains the film at constant thickness. This model may be applicable to the case of the precursor film.

Finally, we note that for a thick enough film, there is the possibility of convection in the the film due to the salty cold liquid overlying hot, fresh liquid. As previously mentioned, we expect the thermal effect to be small relative to the solutal effect due to the high thermal diffusivity relative to solutal diffusivity in the system. In order to estimate the film thickness at which Rayleigh–Benard convection sets in, we approximate the system by Ralyeigh–Benard convection with a solid base and an open top. Letting the critical Rayleigh number be $Ra_c \approx 1000$, and taking the small Peclet number limit (which holds up to films of the order of 1mm thick), we find that [13]

$$Ra_c = \frac{\beta g d^3 (c_T - c_L)}{D_s \nu} \approx 1100\tag{29}$$

where all the symbols take their standard meanings. Thus we expect Rayleigh Benard convection to set in when $d \approx 2mm$.

4 Flow in a thin film

Consider a droplet of salt solution evaporating on an infinite planar substrate. Evaporation is driven by the far–field vapour pressure below the equilibrium vapour pressure of the film. Towards the edge of the droplet, the liquid film is exposed to the drier air above the adjacent dry substrate, while in the centre of the droplet, the ambient air is more moist due to the homogeneity of the environment more than a diffusion length from the edge. This means that the evaporation rate will change from the centre to the edge of the film, and hence there will be a gradient in salinity along the surface of the film and an associated marangoni flow.

The Marangoni effect is a well known process whereby gradients in surfactant concentration in liquids cause associated gradients in surface tension. These gradients then drive

a flow from regions of low surface tension to regions of high surface tension. Unlike for most solutes, where the Marangoni coefficient, or gradient in surface tension associated with a change in solute is negative, for ionic salts such as ammonium chloride and sodium chloride, the surface tension gradient,

$$\frac{\partial \gamma_{lv}}{\partial c} \approx 4 \times 10^{-4} \mathrm{J\,m^{-2}\,wt\%^{-1}} \tag{30}$$

is positive [14]. This means that as the evaporation rate, and hence the salinity, increases towards the edge of the film, we will see an outwards marangoni flow associated with the salinity gradient. We can analyse the flow in order to determine the volume flow rate, and the possibility of this flow as a volume source for precursor film growth.

Assuming that the film is thin enough that we can use lubrication theory, when we incorporate the marangoni flow, the equation of conservation of solute (3) becomes

$$\frac{\partial c}{\partial t} - V\frac{\partial c}{\partial z} + z\frac{\tau}{\mu}\frac{\partial c}{\partial x} = D_s\frac{\partial^2 c}{\partial z^2} + D_s\frac{\partial^2 c}{\partial x^2}, \tag{31}$$

where μ is the dynamic viscosity of water and

$$\tau = \frac{\partial \gamma_{lv}}{\partial c}\frac{\partial c}{\partial x} \tag{32}$$

is the surface stress, and in order to simplify the model, we will assume that the the liquid is a planar film of constant thickness d, and that the surface concentration is linear in x [15], which is equivalent to the assumption that the vapour pressure is linear in x (Fig. 6).

We would like to investigate whether adding a linear surface concentration gradient will significantly vary the concentration profile in the film. Therefore, we will consider the small Peclet number case in the instance that the surface concentration is given by

$$c_T = c_0 + Gx. \tag{33}$$

By imposing this concentration profile, we have also imposed a horizontal lengthscale upon the problem given by $(c_O - c_L)/G$, which we will assume is large relative to d so that we can reduce equation (31) to

$$z\frac{\tau}{\mu}\frac{\partial c}{\partial x} = D_s\frac{\partial^2 c}{\partial z^2},$$

and so upon non–dimensionalisation of lengths with d, and concentrations such that $c = (c_0 - c_L)\tilde{c} + c_L$, the governing equations become

$$\tilde{z}F\frac{\partial \tilde{c}}{\partial \tilde{x}} = \frac{\partial^2 \tilde{c}}{\partial \tilde{z}^2}, \tag{34}$$

with

$$\tilde{c}(0) = 0, \tag{35}$$
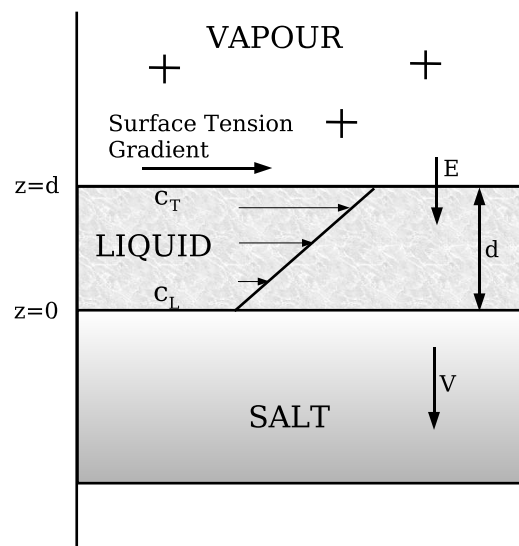
and

$$\tilde{c}(d) = 1 + \delta\tilde{x}, \tag{36}$$

Figure 6: Schematic diagram for a marangoni film in a thin film.

where $F = \tau d^2/\mu D_s$ is the ratio of the diffusive response time to the viscous response time over the film and we have required $\delta = Gd/(c_0 - c_L) \approx GD_s$ to be small as previously mentioned. Estimating $c_0 - c_L = p$ from the small Peclet number, this implies that for typical evaporation rates, $G \ll 2700\text{wt}\%\text{m}^{-1}$, which will be satisfied over all but the very edges of the droplet (see Appendix C).

We proceed by seeking a separable solution to the equations, by setting (dropping tildes) $c(x, z) = X(x)Z(z)$ so that

$$F\frac{X'}{X} = \lambda = \frac{Z''}{Zz}, \tag{37}$$

where λ is a constant. Thus we see that

$$X = Ae^{\frac{\lambda x}{F}},$$

which for small values of the exponent becomes

$$X = A\left(1 + \frac{\lambda x}{F}\right)$$

which is of the right form to match Eq. (36) if we set $\lambda/F = \delta$, so that our assumption of a small exponent value is appropriate for $\delta x \ll 1$.

Thus we see that

$$Z'' - \frac{d^3\tau G}{\mu D_s(c_0 - c_I)}zZ,$$

and by letting $z = \alpha\zeta$, with

$$\alpha = \left(\frac{\mu D_s(c_0 - c_I)}{d^3\tau G}\right)^{\frac{1}{3}},$$

the Z equation reduces to Airy's Equation

$$Z''(\zeta) - Z(\zeta)\zeta = 0. \tag{38}$$

Therefore we find the dimensional solution to the concentration profile to be

$$\begin{aligned}
c &= c_I + (c_0 - c_I)\left[\frac{\text{Bi}\left(\frac{z}{\alpha d}\right)\text{Ai}(0) - \text{Ai}\left(\frac{z}{\alpha d}\right)\text{Bi}(0)}{\text{Bi}\left(\frac{1}{\alpha}\right)\text{Ai}(0) - \text{Ai}\left(\frac{1}{\alpha}\right)\text{Bi}(0)}\right]e^{\frac{Gx}{(c_0 - c_I)}} \tag{39}\\
&= c_I + (c_0 - c_I)f(z)e^{\frac{Gx}{(c_0 - c_I)}}
\end{aligned}$$

Thus we see that the relative importance of the Marangoni flow is given by the size of the parameter α: when α is large, we can Taylor expand Eq. (39) to see that

$$c \approx c_I + (c_0 - c_I)\frac{z}{d}e^{\frac{Gx}{(c_0 - c_I)}} \approx c_I + (c_0 - c_I + Gx)\frac{z}{d}$$

so that we may effectively ignore the horizontal flow, and treat the concentration profile as linear. However, when α is sufficiently small, the solution can deviate from the linear solution.
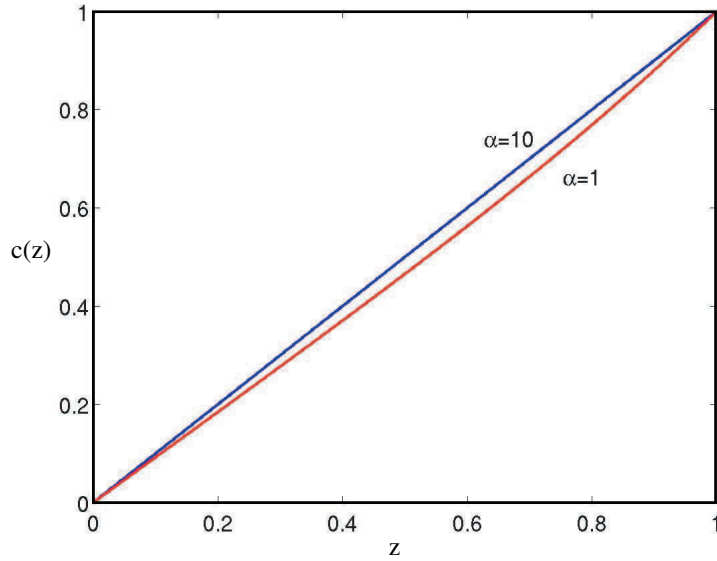
218

Figure 7: $f(x)$ calculated for $\alpha = 1, 10$. To good approximation $c = z/d$ for $\alpha > 1$.

In Appendix C, we treat the question of the value of G for an evaporating droplet, from which we obtain a reasonable upper estimate for G near the edge of the droplet of $2.7 \times 10^3 \text{wt}\%\text{m}^{-1}$. For films in the small Peclet number limit, this implies $\alpha \gg 1$ except within $2d$ of the edge of the droplet where geometry dependent factors will be important. Therefore there will be no significant alteration to the linear profile across the bulk of the film (cf Fig. 7).

5   Linear stability of a film including marangoni flow

In the previous section, we investigated the concentration profile for a film with a concentration gradient applied to the upper surface giving rise to a Marangoni flow. As has been seen previously, the underlying salt–crystal growth is diffusively unstable, and so the solid–liquid boundary will become corrguated. When we include a Marangoni flow with the perturbation, we expect the perturbation to move upstream because the flow will compress the solutal boundary layer on the upstream side, and thus promote growth in that direction. We can analyse this effect as follows.

From the previous section we saw that the steady state solutal profile for small Peclet number can be closely approximated by

$$c = c_L + (c_0 - c_L)\frac{z}{d}e^{\frac{Gx}{(c_0 - c_L)}}, \tag{40}$$

for $Gx/(c_0 - c_L) \ll 1$. Hence we will use the linear approximation throughout.

Assuming that we are in the lubrication limit and that any perturbations are long wavelength, the non–dimensional governing equations are the same as previously (Eqns. 34-36). Therefore the steady state can be taken as that given in Eqn. (40).

If we apply a perturbation of the form

$$z = \tilde{h}e^{ik\tilde{x}+\sigma t}$$

to the solid–liquid interface (where we do not expect σ to be real), then $\tilde{c} = c_0(\tilde{x}, \tilde{z}) + \bar{c}(\tilde{z})exp(ik\tilde{x} + \sigma t)$, where c_0 is the steady state solution. Neglecting the Gibbs–Thomson effect, and dropping tildes we find that

$$ikF\bar{c} = \bar{c}'', \tag{41}$$

and we can convert this to Airy's equation by transforming

$$z = i \left(\frac{1}{kF} \right)^{\frac{1}{3}} \zeta \equiv i\beta\zeta.$$

Thus

$$\bar{c} = -\tilde{h} \left[\frac{\text{Ai}\left(\frac{z}{i\beta}\right) \text{Bi}\left(\frac{1}{i\beta}\right) - \text{Ai}\left(\frac{1}{i\beta}\right) \text{Bi}\left(\frac{z}{i\beta}\right)}{\text{Ai}(0)\text{Bi}\left(\frac{1}{i\beta}\right) - \text{Ai}\left(\frac{1}{i\beta}\right) \text{Bi}(0)} \right], \tag{42}$$

and by applying the boundary condition for conservation of salt (Eqn. 6), we obtain the dispersion relation for the system

$$\sigma = \frac{iD_s}{\beta d^2} \left(\frac{c_L - c_0}{1 - c_L} \right) \left[\frac{\text{Ai}'(0)\text{Bi}\left(\frac{1}{i\beta}\right) - \text{Ai}\left(\frac{1}{i\beta}\right) \text{Bi}'(0)}{\text{Ai}(0)\text{Bi}\left(\frac{1}{i\beta}\right) - \text{Ai}\left(\frac{1}{i\beta}\right) \text{Bi}(0)} \right]. \tag{43}$$

Figure 8 shows the imaginary part of σ, as a function of β. As expected, the velocity of the travelling waves disappears for small k (large β), and we see that σ is significant relative to the timescale V/d associated with the growth of the salt for $\beta < 1$. From the previous linear stability analysis, we found that the most unstable wavenumber was $k_{max} \approx 3.57 \times 10^5 d$, which corresponds to $\beta = (1.2 \times 10^{-14}/d^3G)^{1/3}$ and therefore we see from the appendix estimates of G that the travelling velocity of the waves may be significant for sufficiently thick films.

It should be mentioned that this is only a longwave analysis of the problem, and for k small, the entire Laplacian must be considered in Eq. (34). This will also reintroduce the instability considered in the first linear stability analysis. However this analysis should give a good indication of the relative size of the travelling wave velocity.

6   Volume flow rate due to Marangoni flows

We are interested in whether the gradient in surface concentration across a droplet is sufficient to act as a source for precursor film growth. From the Appendix, we have that

$$\frac{\partial c_T}{\partial r} = \frac{2c_I dD_v (P_I - P_\infty)}{\pi D P_a} \frac{r}{(R^2 - r^2)^{\frac{3}{2}}}.$$
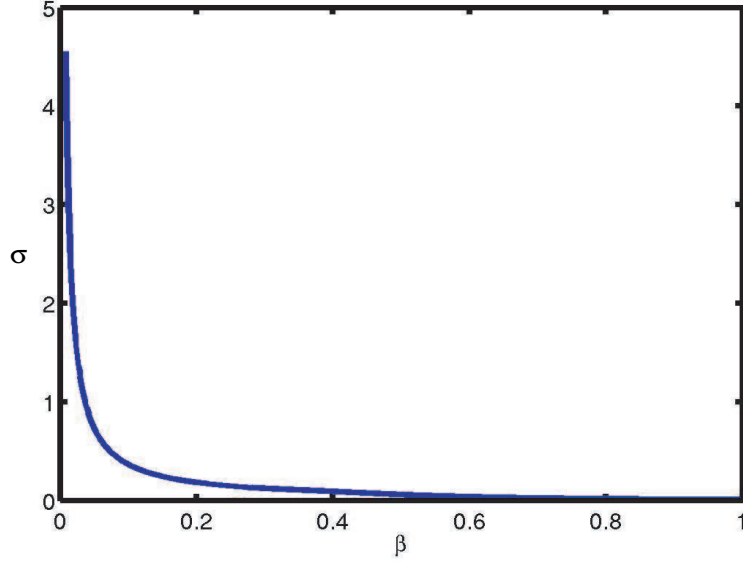
Figure 8: $\text{Im}(\sigma)$ from the dispersion relation for the travelling wave instability in terms of β.

and from lubrication theory, the volumetric flow rate is

$$\int_0^d z \frac{\partial \gamma}{\partial c} \frac{\partial c}{\partial r} \frac{1}{\mu} dz = \frac{d^2}{2\mu} \frac{\partial \gamma}{\partial c} \frac{\partial c}{\partial r}.$$

so that the flow rate is given by

$$q = \frac{c_I d^3 D_v (P_I - P_\infty)}{\pi \mu D P_a} \frac{\partial \gamma}{\partial c} \frac{r}{(R^2 - r^2)^{\frac{3}{2}}}. \tag{44}$$

As discussed in the Appendix, we will ignore the region at the edge of the droplet, as there will be local shape complications there that will effect the expression for c_T. In order to avoid this, we calculate q at a distance d from the edge of the droplet, to find that for $R = 1\text{cm}$, $d = 10^{-6}$ that $q(R - d) \approx 3.4d$ or 1.2cm hr^{-1} which is in line with typical growth rates of the film.

It should be noted that there are only sufficiently large concentration gradients to maintain this flow rate near to the edge of the film. However away from the edge, decreases in curvature associated with the Marangoni flow should draw fluid outwards to help maintain the source of liquid to the edge.

7   Conclusions

In this work, we have considered the processes involved with the growth of salt from an sessile, salty, evaporating droplet. The chief result is that we have demonstrated the existence of a new instability of the growing salt crystal due to evaporation at the liquid–vapour

221

interface. The instability stems from the creation of supersaturation at the evaporating interface, which diffuses through the film to the growing salt crystal. Hence the salt crystal grows into an increasing supersaturation and the interface will be unstable. The instability differs from the morphological instability of a binary alloy [8] in that in the new instability, the creation of supersaturation is created at some distance *away* from the advancing salt front. Whereas with morphological instability, the supersaturation is caused by rejection of solvent immediately adjacent to the salt front.

We find that for typical evaporation rates, the instability will be important for films of thickness $d > 1.5 \times 10^{-5}$m. For sufficiently thick films ($d \sim O(1\text{mm})$), convection will set in and the formulation becomes invalid. Marangoni convection may also be important, as well as thermal effects, howeverthese are expected to be small relative to the solutal effects.

For a growing droplet, there will exist gradients in surface tension associated with the gradient in evaporation rate across the liquid–vapour interface. Associated with these gradients in surface tension there will be a Marangoni flow that drives liquid outwards, feeding the precursor film observed in experiments. We have analysed the effect of the Maragoni flow on solutal profile in the small Peclet number regime (relevant for typical film thicknesses), and find that there will be no significant alteration to the solutal profile across the film except in the tip region, where geometry effects are expected to be important.

We have also analysed the effect of the Marangoni flow upon corrugation of the salt surface. We find that the flow induced compression of the upstream boundary layer of the surface roughness causes increased solid growth thereby creating an upstream travelling solid/liquid wave. The calculated travelling wave velocity suggests that the process will be operative in sufficiently thick films. Finally an estimate of the overall flow rate due to Marangoni flow in a precursor film shows that the flow is sufficient to cause observed spreading rates of the precursor film.

As noted in the text, numerical work is necessary to properly analyse the intermediate Peclet number case and solutal convection, and we hope to achieve these in further studies. For the future, we aim to produce a more complete model of the precursor film including electrostatic double layer forces and van der Waals forces and to extend the results from the current work to produce a more complete model of the processes involved in salty droplet evaporation and salt tree formation.

8   Acknowledgements

9 Appendix A: Derivation of the Gibbs–Thomson co–efficient $\mathcal{C}$

In order to obtain an approximation for $\mathcal{C}$, the dependence of the equilibrium salt concentration at an interface upon curvature, we start with the liquidus relationship at a curved surface including solute:

$$T = T_m - m(1 - c) + \frac{\gamma_{sl} T_m}{\mathcal{L}_f} \mathcal{K} \tag{45}$$

where T_m is the melting temperature of a pure liquid salt, m is the slope of the liquidus, γ_{sl} is the surface energy of the liquid–salt interface and $\mathcal{L}_f$ is the heat of solution of the salt. We note that we have assumed that the curvature term is independent of solution concentration, so the resulting expression will not be exact.

Rearranging, we obtain

$$c = 1 - \frac{T_m - T}{m} - \frac{\gamma_{sl} T_m}{m \mathcal{L}_f} \mathcal{K} \tag{46}$$

we we recognise as

$$c = c_L(T) + \mathcal{C} \mathcal{K} \tag{47}$$

where $c_L(T)$ is the liquidus concentration, so that we find

$$\mathcal{C} = -\frac{\gamma_{sl} T_m}{m \mathcal{L}_f}. \tag{48}$$

Taking typical values of the constants, $\mathcal{L}_f = 4 \times 10^8 \, \mathrm{J\,m^{-3}}$, $T_m = 273\mathrm{K}$ and $\gamma_{sl} = 5 \times 10^{-2} \, \mathrm{J\,m^{-2}}$, we find that $\mathcal{C} \sim -7 \times 10^{-9} \mathrm{wt\%\,m}$.

10 Appendix B: Equilibrium vapour pressure and surface concentration

We consider the effect upon equilibrium vapour pressure of adding salt to a liquid. In equilibrium, the chemical potentials of the two phases are equal:

$$\mu_l(T, P, c) = \mu_v(T, P), \tag{49}$$

where the subscripts correspond to liquid and vapour respectively and we have assumed the vapour pressure of salt to be zero.

Expanding the chemical potentials about pure equilibrium at temperature T and vapour pressure P_0, and using the Gibbs–Duhem equation [Wood Battino],

$$\mu_l(T, P_0) + v_l(P - P_0) - kTc = \mu_v(T, P_0) + v_v(P - P_0), \tag{50}$$

where $v_l \ll v_v$ are the volumes per mole of each phase, so that using

$$\mu_l(T, P_0) = \mu_v(T, P_0), \tag{51}$$

we obtain

$$P - P_0 = -\frac{kT}{v_v} c, \tag{52}$$

which for an ideal gas becomes

$$P = P_0(1 - c). \tag{53}$$

11   Appendix C: Estimating the magnitude of G

For a realistic experiment, the controllable factors are the temperature T, the initial salinity of the droplet, the initial volume of the droplet and the far field water vapour pressure P_∞. Therefore there will be a variation in local vapour pressure at the surface of the droplet which is determined by local equilibrium with the droplet and diffusion in the vapour.

Assuming that the vapour is stagnant above the droplet so that vapour transport occurs by diffusion alone, then the vapour pressure will satisfy Laplace's equation

$$\nabla^2 P = 0. \tag{54}$$

A number of studies [11],[5] have modelled the evaporation rates of a pure droplet by treating the vapour diffusion problem identically to an electrostatic problem. Poulard et al. assumed that the droplet is effectively a flat disc, which is appropriate for fluids with small contact angles to the substrate, while Deegan et al achieved a more accurate result by considering the electrostatic field associated with a lens. As we require an estimate only, we will assume the evaporation rate matchs that for a disc held at constant surface vapour pressure so that the evaporation rate is approximately

$$E \approx \frac{2D_v(P_I - P_\infty)}{\pi P_a} \frac{1}{\sqrt{R^2 - r^2}} \tag{55}$$

where D_v is the diffusion rate of water vapour in the air, P_a is atmospheric pressure, P_I is the vapour pressure for a droplet in equilibrium with the vapour, r is the radial coordinate for the disc, and R is the radius of the disc.

Although in deriving the evaporation rate, we have assumed a constant vapour pressure (and hence constant surface concentration which is only an approximation), this should provide us with a reasonable approximation for the local surface vapour pressure.

We will now convert the local evaporation rate into the surface concentration c_{surf} as follows. Using the boundary condition for conservation of mass at the liquid–vapour interface,

$$D_s \frac{\partial c}{\partial z}\bigg|_{z=d} = Ec_T, \tag{56}$$

and using the approximations

$$c_T = c_L \quad \text{and} \quad \frac{\partial c}{\partial z} = \frac{c_T - c_L}{d}, \tag{57}$$

we find that

$$E = \frac{D_s}{d}\left(\frac{c_T - c_L}{c_L}\right) \tag{58}$$

and so

$$c_T - c_L = \frac{2c_I d D_v(P_I - P_\infty)}{\pi D_s P_a} \frac{1}{\sqrt{R^2 - r^2}}$$

so that

$$\frac{\partial c_T}{\partial r} = \frac{2c_I d D_v(P_I - P_\infty)}{\pi D_s P_a} \frac{r}{(R^2 - r^2)^{\frac{3}{2}}}.$$

As we expect there to be shape determined complications at the edge of the droplet we take $r = R - d$ to obtain an upper limit upon $\mathcal{C}$, and $r = 0$ for a lower limit. Therefore, for a 6% difference in relative humidity so that $(P_I - P_\infty)/P_a \approx 1.8 \times 10^{-3}$, and letting $d = 10^{-6}$m, we find that a reasonable approximation for G is that it will vary from 0 to $2.7 \times 10^3 \mathrm{wt\%\,m^{-1}}$ across the droplet.

References

[1] J. M. Fournier and A. M. Cazabat. Tears of wine. *Europhys. Lett.*, 20:517–522, 1992.

[2] A. E. Hosoi and J. W. M. Bush. Evaporative instabilities in climbing films. *J. Fluid Mechs.*, 442:217–239, 2001.

[3] A. Oron, S. H. Davis, and S. G. Bankoff. Long-scale evolution of thin liquid films. *Rev. Mod. Phys.*, 69(3):931–980, 1997.

[4] P. G. de Gennes. Wetting: statics and dynamics. *Rev. Mod. Phys.*, 57(3):827–863, 1985.

[5] R. D. Deegan, O. Bakajin, T. F. Dupont, Greg Huber, S. R. Nagel, and T. A. Witten. Contact line deposits in an evaporating drop. *Phys. Rev. E*, 62(1):756–765, 2000.

[6] S. G. Lipson. Pattern formation in drying water films. *Physica Scripta*, T67:63–66, 1996.

[7] Rose Du and H. A. Stone. Evaporatively controlled growth of salt trees. *Phys. Rev. E*, 53(2):1994, 1996.

[8] M. G. Worster. Solidification of fluids. In G. K. Batchelor, H. K. Moffat, and M. G. Worster, editors, *Perspectives in Fluid Dynamics*. Cambridge University Press, 2000.

[9] W. W. Mullins and R. F. Sekerka. Stability of a planar interface during solidification of a dilute binary alloy. *J. Appl. Phys.*, 35(2):444, 1964.

[10] H. E. Huppert. The fluid mechanics of solidification. *J. Fluid Mechs.*, 212:209, 1990.

[11] C. Poulard, G. Guena, and A. M. Cazabat. Diffusion–driven evaporation of sessile drops. *J. Phys. Condens. Matt.*, 17(49):S4213–S4227, 2005.

[12] V. P. Skripov and M. Z. Faizullin. *Crystal–Liquid–Gas Phase Transitions and Thermodynamic Similarity*. Wiley, 2006.

[13] J. S. Turner. *Buoyancy Effects in Fluids*. Cambridge University Press, 1973.

[14] S. A. Lowry, M. H. McCay, T. D. McCay, and P. A. Gray. Surface–tension measurements of aqueous ammonium chloride (NH_4Cl) in air. *J. Cryst. Growth*, 96(4):774–776, 1989.

[15] J. S. Wettlaufer, M. Elbaum, H. A. Stone, and M. G. Worster. Molecular diffusion in nonequilibrium alloy films and molecular motion in polymeric networks. In D. C. Gillies and D. E. McCauley, editors, *Proceedings of the NASA Microgravity Materials Science Conference, Huntsville, Alabama, 14-16 July*, pages 679–684. NASA/CP-1999-209092, 1999.